Naval Research Laboratory

Washington, DC 20375-5320

NRL/MR/6362--20-10,156

Low-pressure Chemical Vapor Deposition of Graphene Films on Copper Foils

Evgeniya H. Lock

Materials and Sensors Branch
Materials Science and Technology Division

Sandra M. Rodriguez

SSEP-STEM Student from University of Puerto Rico
San Juan, PR

Daniel S. Choi

NRC Postdoctoral Researcher
Washington, DC

November 30, 2020

REPORT DOCUMENTATION PAGE

Form Approved
OMB No. 0704-0188

1. REPORT DATE *(DD-MM-YYYY)*	**2. REPORT TYPE**	**3. DATES COVERED** *(From - To)*
30-11-2020	NRL Memorandum Report	01 Oct 2019 – 30 Sep 2020

4. TITLE AND SUBTITLE

Low-pressure Chemical Vapor Deposition of Graphene Films on Copper Foils

5a. CONTRACT NUMBER

5b. GRANT NUMBER

5c. PROGRAM ELEMENT NUMBER

6. AUTHOR(S)

Evgeniya H. Lock, Sandra M. Rodriguez*, and Daniel S. Choi**

5d. PROJECT NUMBER

5e. TASK NUMBER

5f. WORK UNIT NUMBER
1G71

7. PERFORMING ORGANIZATION NAME(S) AND ADDRESS(ES)

Naval Research Laboratory
4555 Overlook Avenue, SW
Washington, DC 20375-5320

8. PERFORMING ORGANIZATION REPORT NUMBER

NRL/MR/6362--20-10,156

9. SPONSORING / MONITORING AGENCY NAME(S) AND ADDRESS(ES)

10. SPONSOR / MONITOR'S ACRONYM(S)

11. SPONSOR / MONITOR'S REPORT NUMBER(S)

12. DISTRIBUTION / AVAILABILITY STATEMENT

DISTRIBUTION STATEMENT A: Approved for public release; distribution is unlimited.

13. SUPPLEMENTARY NOTES

*SSEP-STEM Student, 4555 Overlook Ave., S.W., Washington, DC 20375-5320
**NRC Postdoctoral Researcher, 500 Fifth Street, N.W., Washington, DC 20001

14. ABSTRACT

Graphene is a novel two-dimensional material with great potential for electronic applications due to its exceptional electrical properties such as extremely high electron mobility of 200,000 $cm^2V^{-1}s^{-1}$and carrier concentration of 10^{12} cm^{-2}. Thus, the potential of graphene for applications in many technologies such as flexible electronic devices, chemical and biological sensors, energy storage devices, etc. has been successfully demonstrated in laboratory settings. However, before technological applications of graphene can be realized, cost-effective, highquality, large-scale production is necessary. Low-pressure chemical vapor deposition (LPCVD) growth of graphene on copper foils offers a technologically promising approach for this endeavor. However, while highly encouraging, there is still a critical need to tune and optimize the method to produce large grains and reduce graphene film defects. In this work, we provide a comprehensive study on the effects of different parameters such as substrate type, time, temperature, pressure, and gas flow rates for each synthesis step on the final graphene film quality. Extensive surface characterization was performed using optical microscope imaging and Raman spectroscopy. The impact of this work is to provide a correlation between the growth parameters and the chemical, structural, and morphological properties of graphene films grown on copper foils.

15. SUBJECT TERMS

Graphene Growth
Raman spectroscopy Optical microscopy

16. SECURITY CLASSIFICATION OF:			**17. LIMITATION OF ABSTRACT**	**18. NUMBER OF PAGES**	**19a. NAME OF RESPONSIBLE PERSON**
a. REPORT	**b. ABSTRACT**	**c. THIS PAGE**			Evgeniya H. Lock
Unclassified Unlimited	Unclassified Unlimited	Unclassified Unlimited	Unclassified Unlimited	28	**19b. TELEPHONE NUMBER** *(include area code)* (202) 767-0351

Standard Form 298 (Rev. 8-98)
Prescribed by ANSI Std. Z39.18

This page intentionally left blank.

Low-Pressure Chemical Vapor Deposition Growth of Graphene Films on Copper Foils

Sandra M. Rodriguez[1], Daniel S. Choi[2,] and Evgeniya H. Lock[3]

[1]SSEP-STEM Student from the University of Puerto Rico in residence at the Naval Research Laboratory, Washington DC 20375

[2]National Research Council Postdoctoral Fellow in residence at the Naval Research Laboratory, Washington DC 20375

[3]Materials Science and Technology Division, Naval Research Laboratory, Washington DC 20375

Abstract

Graphene is a novel two-dimensional material with great potential for electronic applications due to its exceptional electrical properties such as extremely high electron mobility of 200,000 $cm^2V^{-1}s^{-1}$ and carrier concentration of 10^{12} cm^{-2}. Thus, the potential of graphene for applications in many technologies such as flexible electronic devices, chemical and biological sensors, energy storage devices, etc. has been successfully demonstrated in laboratory settings. However, before technological applications of graphene can be realized, cost-effective, high-quality, large-scale production is necessary. Low-pressure chemical vapor deposition (LPCVD) growth of graphene on copper (Cu) foils offers a technologically promising approach for this endeavor. However, while highly encouraging, there is still a critical need to optimize the method to produce high quality graphene film with minimal defects. In this work, we provide a comprehensive study on the effects of growth parameters such as time, temperature, pressure, and gas flow rates for each synthesis step as well as Cu foil purity on the graphene film quality. Extensive surface characterization was performed using optical microscope imaging and Raman spectroscopy. The impact of this work is to provide a correlation between the growth parameters and the chemical, structural, and morphological properties of graphene films grown on copper foils.

I. Introduction

a) Applications of graphene

Graphene is a one-atom-thick, two-dimensional (2D) material with a structure consisting of sp^2 hybridized carbon atoms. A honeycomb arrangement of three unpaired electrons form σ-bonds with neighboring carbon atoms along the horizontal plane. In contrast, the fourth π electron is delocalized around the ring structures along the vertical plane. This molecular structure allows for the unbound π electrons to move freely and quickly across the lattice, thus allowing graphene to be an excellent electrical conductor with the highest known electron mobility of 200,000 $cm^2V^{-1}s^{-1}$, which is one hundred times greater than that of silicon and with a carrier concentration of 10^{12} cm^{-2} [1]. Additionally, due to its Dirac cone band structure, where conduction and valence bands meet at a single sharp point, graphene is a zero bandgap, semi-metal with the ability for ballistic transport of electrons[2].

Manuscript approved November 23, 2020.

These exceptional electronic properties have made graphene a very attractive material for many electronic, optoelectronics, energy storage, and sensing applications. The high electron mobility in graphene makes it an excellent candidate for high-speed electronics to produce the next generation ultrathin transistors[3–5]. In addition, graphene allows for longer charge separation combined with very high transport velocity making possible applications in ultrafast and efficient photodetectors[6,7], optical modulators[8], plasmonic structures[9], and waveguides[10–13]. Furthermore, the high optical transparency and electrical properties of monolayer graphene make it an ideal material for electrical contacts in solar cell technology[14,15], displays, and conductive electrodes[16,17].

As a two-dimensional material, graphene has a very high surface area of 2,630 m^2/g[16] leading to record-breaking capacity storage in graphene supercapacitors. Graphene has also been used in lithium-ion batteries. Its incorporation in the anode improves the battery charging and recharging rates due to the increased surface area allowing for fast redox reactions[18]. The large surface area leads to the extreme sensitivity of graphene chemical, biological, radiological sensors. For example, graphene gas phase sensors can detect single molecules. Graphene's biosensors can detect specific peptides, antibodies, DNA, cells, and cancer biomarkers[19–22]. Also, electrochemical sensors are capable of detecting heavy metal ions with nanomolar limits of detection in soil and water[16,23].

Despite these advantages that graphene offers across many applications, manufacturing large-scale, low-cost, high-quality material is still challenging as precise control of the growth conditions is required. While many different synthesis methods have been developed over the years, limitations in the techniques, as well as the scale and the quality of the resulting product, have led to bottlenecks in the usage of graphene in mass production. The next section discusses the past graphene synthesis efforts and presents an alternative method for producing high-quality graphene films that is also economically promising.

b) Graphene synthesis methods

There have been many graphene synthesis methods explored to achieve large scale high-quality graphene films. Some of these methods include exfoliation[24], combustion[25], epitaxial growth[26], and chemical vapor deposition (CVD)[27,28], as shown in Figure 1. While successful synthesis of graphene has been achieved by the methods mentioned above, each method has drawbacks that stagnate the progress and limit usage to the laboratory or small-scale settings.

The traditional exfoliation or "scotch tape method", is achieved via mechanical cleavage of graphene films and crystals from larger carbon allotropes such as bulk graphite[24]. While this method is facile and the produced graphene crystals have high quality, the approach is not technologically relevant. As such, the synthesis of graphene has moved towards a bottom-up approach through chemical reactions.

In combustion synthesis of graphene, an oxygen-ethylene gas mixture is injected into a hydrostatic column and ignited to over 4,000 K to drive combustion reactions to produce graphene[25]. Additionally, metals such as magnesium or calcium are combusted in the CO_2 atmosphere to produce graphene films with fewer than ten layers (metal oxides are byproducts of these reactions)[29,30]. While the combustion process is quick, it is difficult to control, it requires high temperature to operate, and the synthesized graphene is non-uniform. Furthermore, often low-quality product results which limits the use of this method for mass production.

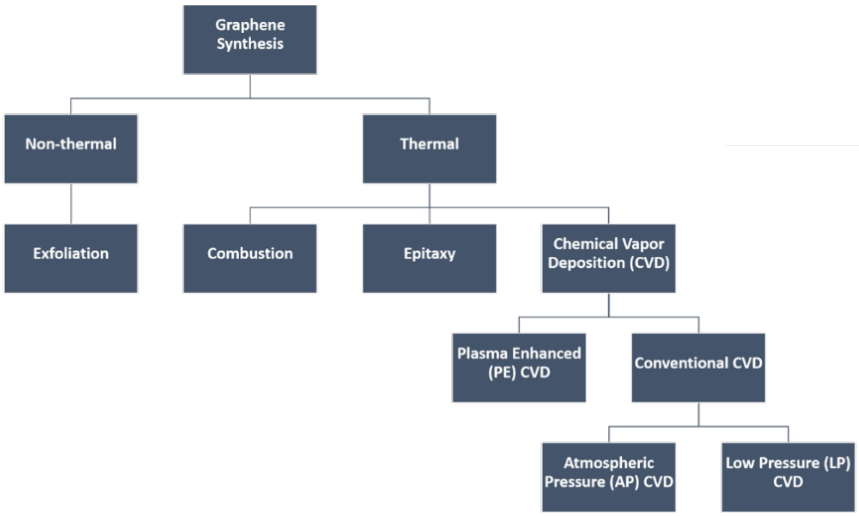

Figure 1. Summary of graphene synthesis methods.

Epitaxial growth of graphene on silicon carbide (SiC) substrates has demonstrated the production of wafer-scale graphene films. In this method, the SiC substrate is heated to a high temperature (> 1,200 ^{o}C) in an argon environment. At these conditions, the carbide decomposes, Si atoms evaporate while carbon atoms recombine to form graphene. The resulting graphene is of high quality with promising electronic properties - carrier mobility of 2.5 x 10^4 $cm^2V^{-1}s^{-1}$ has been reported, making this material highly promising for technological applications. However, even though SiC is a material highly compatible with electronic circuits[31,32], due to the high costs of SiC wafers, this growth approach is used sparingly.

Chemical vapor deposition (CVD) growth of graphene films on metal substrates is the preferred facile, low-cost method for producing high-quality graphene at technologically relevant scales. The CVD growth methods can be divided into two categories depending on the growth temperature: (1) low temperature - plasma-enhanced (PE)CVD and (2) high temperature (conventional) CVD. Generally, in the CVD growth approach, a precursor hydrocarbon gas, such as methane (CH_4), is decomposed and deposited onto the surface of metallic substrates such as nickel (Ni) or copper (Cu) to produce graphene films. In PECVD, as the name suggests, plasma source such as microwave or arc discharge is utilized to break the precursor gas and thus to drive the graphene forming reactions to lower the growth temperature almost by a factor of two (< 700 ^{o}C)[33,34] However, adding a plasma source makes the overall cost of the growth system more expensive than conventional CVD technology.

Additionally, the latter requires a simpler setup of only a tube furnace, and it can produce high-quality large-scale graphene films. Thus, it has demonstrated great potential to meet the industry standards for graphene mass production. Another classification between the CVD growth methods is based on growth pressure: atmospheric (760 Torr) versus low pressure (mTorr range). Of these methods, the low-pressure (LP)CVD is preferred because the lower system pressure allows for better gas control, reduces unwanted gas-phase reactions, and minimizes the nuclei density resulting in larger graphene grains[35,36]. LPCVD is also independent of atmospheric conditions such as air humidity and therefore produces consistently high-quality films. The graphene films produced in this work are via LPCVD, and thus only the low-pressure mechanism is discussed below.

c) Low-Pressure graphene growth mechanism

Low-Pressure Chemical Vapor Deposition (LPCVD) growth of graphene crystals and films can be broken down into three main phases as shown in Figure 2: (i) catalytic decomposition & adsorption of gases, (ii) nucleation of carbon atoms on the substrate surface, and (iii) expansion of graphene nuclei into crystals and films and self-termination. As described in the previous section, graphene is synthesized on nickel and copper substrates because they provide the catalytic effect of breaking down hydrocarbon molecules to grow on the surface[37]. While other transition metals such as palladium, rubidium, and iridium have exhibited the same catalytic effect, nickel and copper are preferred due to their low cost and wide availability[38]. In addition to their catalytic effect, another driving factor in graphene synthesis on metal is the substrates' carbon solubility. As hydrocarbon is decomposed into carbon atoms at high temperature in the presence of a catalyst, carbon atoms will start to adsorb on the metallic substrate (Figure 2i). However, as thinner deposition, i.e., mono- to a few layers of carbon atoms is preferred, excess carbon atoms can adsorb on the metal resulting in unwanted deposition of thick, multilayered carbon structures. Usually, thicker graphene films are grown on Ni, and thinner graphene films and crystals are grown on Cu substrates.

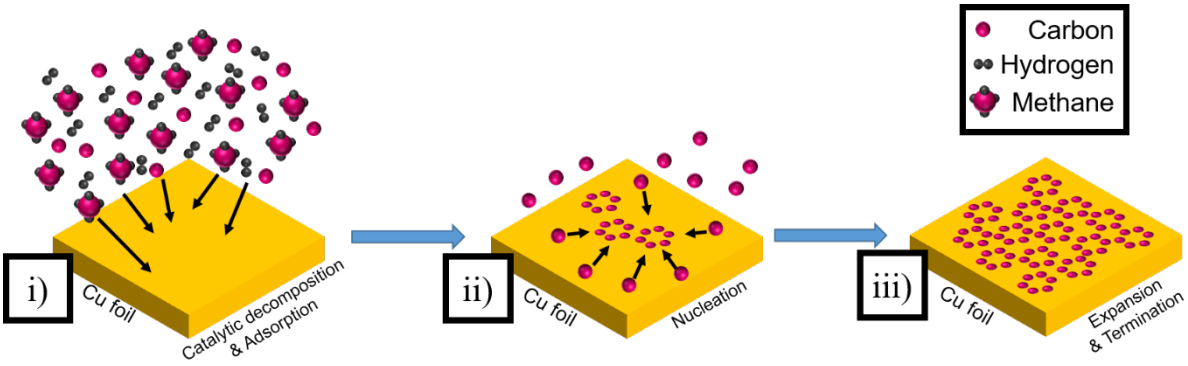

Figure 2. Schematic showing the growth mechanism of graphene on Cu foil by the low-pressure chemical vapor deposition (LPCVD) method: (i) Catalytic decomposition & adsorption of carbon atoms on the Cu surface, (ii) Nucleation of carbon atoms on the Cu surface forming graphene, (iii) Expansion of hexagonal graphene structure until self-terminated.

Figure 3 shows the equilibrium phase diagram of the copper-carbon binary system and explains the above-stated phenomenon: copper has very low carbon solubility of 0.0006 atomic percentage (at. %) at 1,000 ^{o}C,[39] which is significantly lower than its solubility in nickel, which is 1.1 at. % at 1,000 ^{o}C [40]. This ten thousand times lower solubility of carbon into copper means that the excess carbon will not further absorb into the substrate, and the over-deposition of carbon atoms is prevented resulting in self-limiting graphene film growth[41]. As a result, the nucleated carbon atoms (Figure 2ii) will combine in the lateral direction to form hexagonal graphene crystal structures. As the reaction progresses further, the hexagonal crystals will expand throughout the substrate boundary until a uniform film is formed (Figure 2iii)[37]. Depending on the growth conditions, single, bilayer, and trilayer films have been reported[42,43].

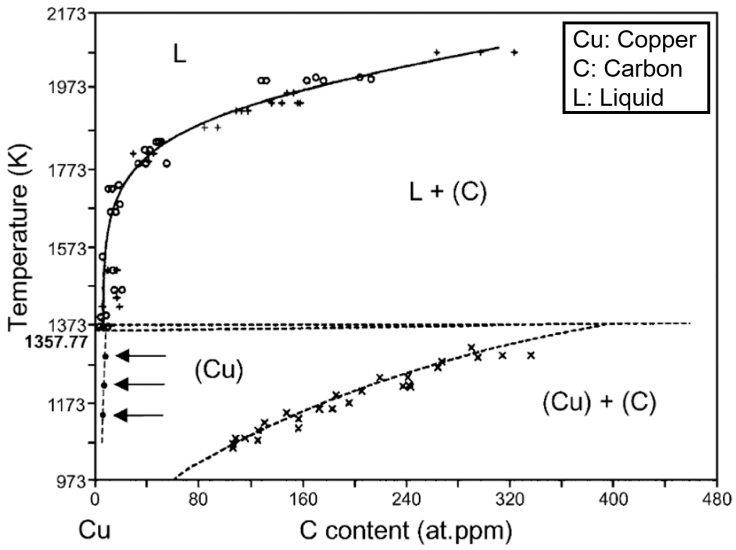

Figure 3. Equilibrium phase diagram of the copper-carbon binary system. At 1000ºC (1273 K), the carbon solubility is 0.0006 at%[39].

A complete LPCVD process includes three main steps - annealing, growth, and cooling. Furthermore, the surface characteristics of the foils, such as purity, surface roughness, and surface defects, influence the graphene films quality to a great extent. Thus, a careful analysis of each step from substrate selection and preparation to annealing, growth, and cooling needs to be optimized independently to achieve uniform, large-area, defect-free growth of graphene films on the copper substrate. In the paragraphs below, the objective of each step and its importance based on available literature data are discussed.

First, the purpose of the substrate preparation step is to eliminate the copper oxide defects from the surface. Some studies have used chemical treatments like acetone, isopropanol, and acetic acid to clean the surface and remove any dust or oxide particles. Additionally, electropolishing of the copper surface has been utilized to reduce the surface roughness and remove the top layer impurities and surface defects[44].

Next, an annealing step is applied to the copper substrate to reduce the surface roughness further, increase grain size, and remove impurities by burning them off at high temperatures. The high temperature allowed the recrystallization of the substrate surface and increased grain size[35,45]. This thermal process is carried out in a hydrogen (H_2) and argon (Ar) atmosphere at temperatures greater than 980 ºC. However, caution must be applied to prevent the phase change of the copper substrate from solid to liquid phase, as described in Figure 3. In this step, the annealing temperature, time, and the ratio of argon and hydrogen gases are varied among researchers and their systems.

Graphene growth is then done at high temperatures with a hydrocarbon source in either the gas or solid phase. Methane is the most commonly used hydrocarbon source[46–48]. However, alcohol vapors such as methanol, ethanol, and propanol[49], as well as other organic solvents such as acetylene[50] and hexane[51]. Solid-state precursors such as PMMA/polystyrene precursor[52] and naturally derived carbon sources from food, insects, and waste[53] have also been utilized. However, methane is the most ubiquitous carbon source due to wide availability, low cost, and the facile mechanism of decomposition from molecular structures to carbon atoms. In addition to

hydrocarbon source selection, the hydrogen carrier gas is incorporated to help initiate the graphene growth and act as an etching agent to control the size and morphology of the grains and should be monitored as well[54]. Upon completion of the growth, the hydrocarbon source is turned off. The system is rapidly cooled to room temperature under a hydrogen atmosphere at low pressure as fast cooling provides higher quality graphene[55,56].

The objective of this work is to develop systematic protocols for LPCVD synthesis of graphene films on copper foils with large grains and minimal structural defects. The approach taken to this end is to optimize each step of the graphene growth process: (1) the copper film purity and roughness; (2) annealing parameters, and (3) growth parameters including temperature, internal chamber pressure, gas flow rates, and reaction times. A furnace with high-speed cooling was explicitly selected for the graphene film growth, and thus this step was not modified. After each step, the metal copper foils or graphene films on copper foils were characterized by optical microscopy and Raman spectroscopy to qualitatively and quantitatively validate the optimization protocols.

II. Materials and methods

Three copper (Cu) foil substrates with a thickness of 0.025 mm with purities of 99.999 %, 99.98 %, and 99.8 % were used in this work. The Cu foils with purities of 99.999 % and 99.8 % were obtained from Alfa Aesar. The Cu foil with 99.98 % purity was purchased from Sigma Aldrich. All foil samples were cut into 1x1 cm^2 squares before growth. Two methods for surface treatment of the Cu foils were used to reduce the surface roughness of the substrates: chemical treatment with acetic acid and electropolishing. In the first case, the Cu foils were cleaned using the following steps: (1) acetone rinse, (2) deionized (DI) water rinse, (3) acetic acid incubation, followed by (4) isopropanol rinse, and (5) drying under nitrogen gas flow. In the second case, the 99.8 % Cu substrate was electropolished with the Lectropol-5 Automatic Electropolishing Unit (Struers) using an in-house prepared electrolyte to drive the redox reaction. The electrolyte mixture was prepared by first dissolving I-water, phosphoric acid, ethanol, and isopropanol in the following ratios 10:5:5:1. Then, 3.3 g of urea was added to the solution and completely dissolved. Electropolishing was performed using a voltage potential of 8 V for 90 seconds.

All annealing and growth experiments were performed in the MTI OTF-1200X one-temperature zone chemical vapor deposition (CVD) reactor equipped with a 4” diameter quartz tube. The gas pressure and flow were controlled by an MTI double stage mechanical vacuum pump and an MKS type 247 gas flow controller, respectively. The rapid cooling was achieved using the MTI KJ 5000 water recirculation chiller and two fans at both reactor flanges. All CVD reactor components are shown in Figure 4.

The general process for the graphene growth is as follows: (1) the Cu foils were placed on the holder inside the tube (which holder accommodate substrates as large as 3” wafers), (2) the tube end was closed, and the tube was evacuated to a pressure of 6 mTorr, (3) the annealing and growth parameters (time, and temperature) were adjusted in the MTI proprietary software, (4) the pressure and flow rates of the gases (argon for annealing, methane, and hydrogen for growth) were controlled using the mass flow controller and vacuum valve, (5) the chiller was turned on and its setting adjusted before the experiment, (6) after the growth was completed, the samples were cooled under convection with the two fans to facilitate the cooling process, (7) when room temperature was reached, the gases were turned off, the vacuum valve was closed and the system was brought up to atmospheric pressure, (8) the graphene on Cu foil samples were removed and

characterized. The latter was achieved using an Olympus BX53M optical microscope to observe any visible impurities and surface defects. Additionally, Raman analysis was utilized to verify signature G, D, and 2D graphene bands. The G band, located around 1,580 cm^{-1}, shows a molecular picture of the carbon structure resulting from the in-plane vibrational mode of sp^2-hybridized carbon atoms. The D band, also known as the disorder or defect band, results from the ring breathing mode from sp^2 carbon rings near an edge or defect and is present at around 1,350 cm^{-1}. Lastly, the 2D, or second-order overtone of D, band is observed in monolayer graphene with the intensity decreasing as the number of graphene layers increases and is present at around 2,690 cm^{-1}. Raman analysis was performed directly on graphene on copper using a Renishaw inVia Raman Microscope equipped with a 514 nm laser. The spectra were taken between 1,000 cm^{-1} to 3,500 cm^{-1} wavenumber Raman shifts with the characteristic graphene peaks identified.

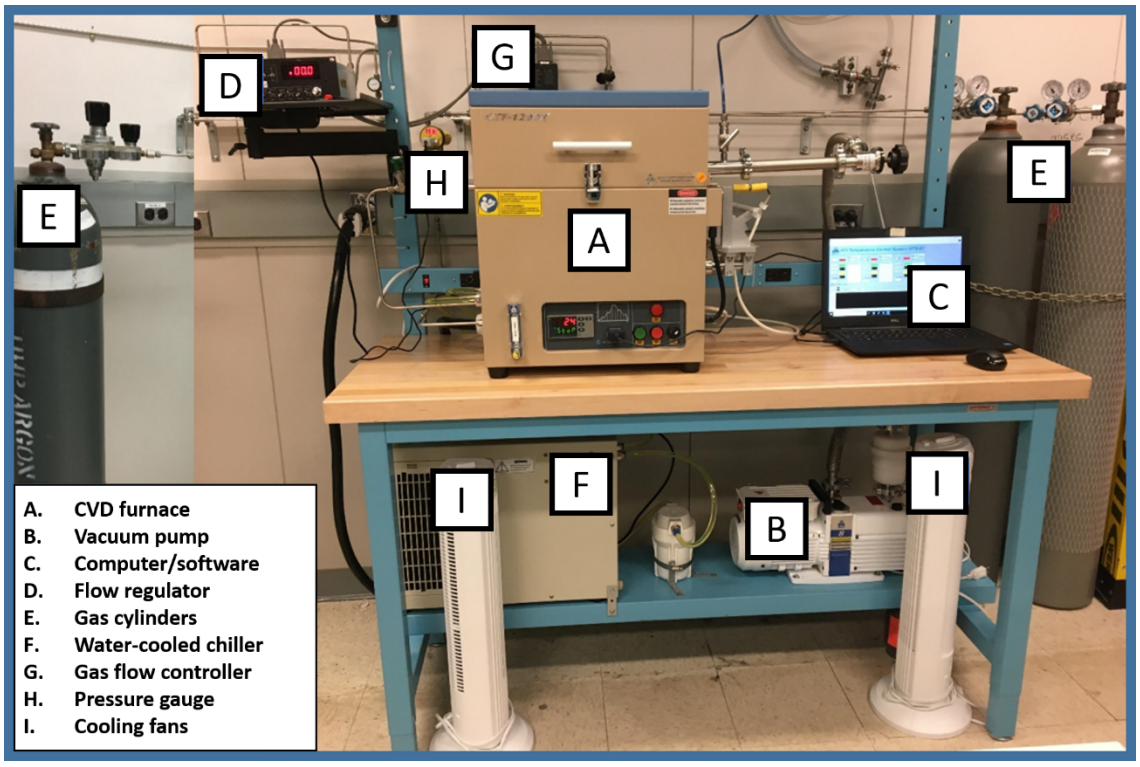

Figure 4. Chemical Vapor Deposition system used for graphene growth. The components are (A) CVD furnace, (B) Vacuum pump, (C) Computer/software, (D) Gas flow regulator module, (E) Gas cylinders, (F) Water-cooled chiller, (G) Gas flow controller, (H) Pressure gauge and (I) Cooling fans.

III. Results and discussion

In the sections below, we describe the optimization of (1) substrate preparation, (2) annealing, and (3) growth conditions in the LPCVD process.

a) Substrate preparation

Figure 5 shows microscope optical images of Cu foil substrates with different purity levels before and after chemical treatment (outlined in the previous section) to analyze copper boundary grains, surface roughness, and surface defects. The lower purity foils 99.98 % and 99.8 % (Figures 5b, 5e, and 5c, 5f respectively) were affected by the chemical treatment as signified by the removal of black spots, deepened trenches, etc., the quality of the 99.999 % purity foil was not improved. Overall, the images also indicate that the surface roughness of this foil was the lowest and thus might have the best potential for graphene growth. Therefore, the 99.999 % Cu foil substrate was used without chemical treatments (only a solvent rinse was applied) for graphene growth. Figure 6 shows the result of an electropolishing treatment on the lowest purity copper substrate (99.8 %). A significant smoothing of the surface was observed, and thus electropolishing is a better solution for achieving smooth surface of the copper foil for low purity Cu foils.

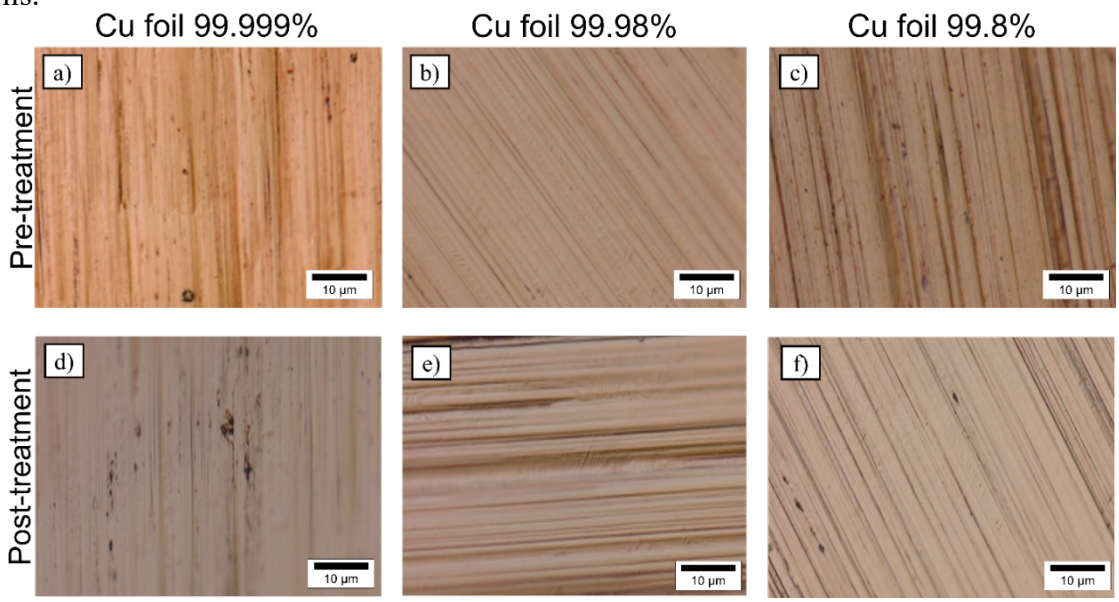

Figure 5. Copper foils of 99.999 %, 99.98 %, and 99.8 % purities before (a, b, c) and after (d, e, f) chemical treatment with acetic acid.

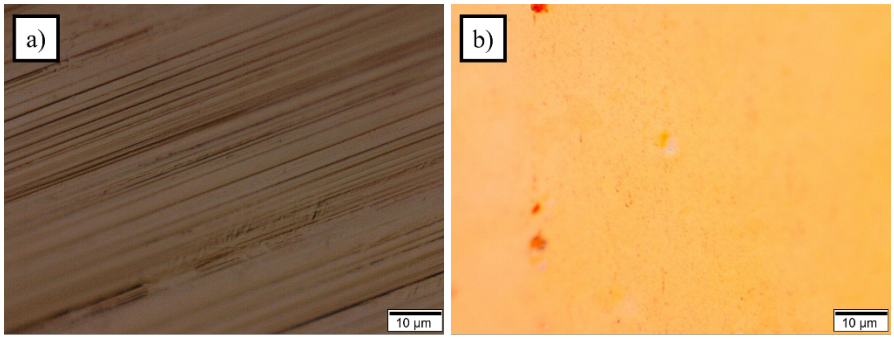

Figure 6. Copper foil of 99.8 % purity before (a) and after (b) electropolishing treatment.

b) Copper substrate annealing results

The untreated, highest purity copper foil (99.999 %) was selected for annealing. Two different sets of annealing experiments were performed to determine the optimal annealing conditions. The first experiment set investigated the effects of temperature, while the second experiment set probed the effects of annealing time on the quality of the copper surface. The goal of the annealing step is to reduce the Cu foil surface roughness and increase its grain size. The exact experimental conditions for both sets are outlined in Table 1.

Table 1. Summary of experimental conditions used for annealing of 99.999 % purity copper foil substrates. Note: the symbol (*B) indicates figures are presented in the appendix.

Figure	Gas Flow (sccm)		Temperature (°C)	Time (min)	Pressure (mTorr)
	H_2	Ar			
5a	2	5	900	20	260-382
*C	2	5	900	20	5000-10000
5b	2	5	950	20	189-382
5c	2	5	970	20	219-388
5d	2	5	980 - 1000	10 - 10	260-380
6a	2	5	970	40	256-358
6b	2	5	970	60	219-359
*B	2	5	980	60	199-362
6c	2	5	970	90	223-332
6d	2	5	970	120	220-335
*B	2	5	960	120	255-352

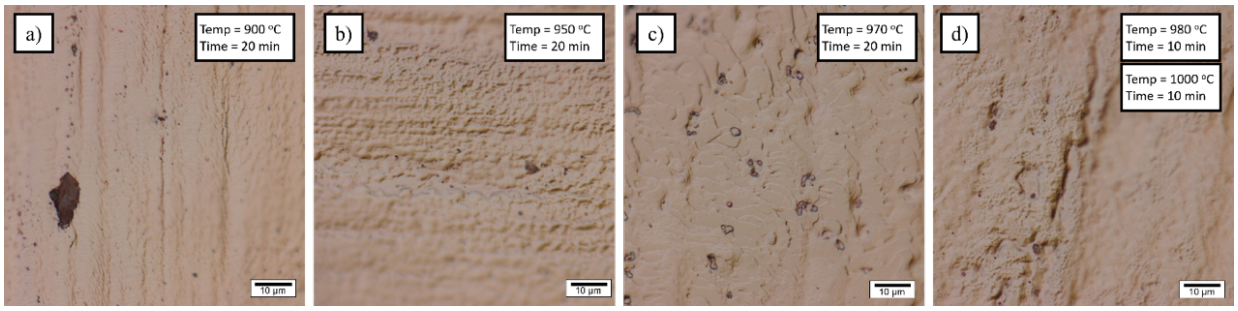

Figure 7. Copper foil after annealing experiments at different temperatures: (a) 900 °C, (b) 950 °C, (c) 970 °C and (d) 980 °C/1,000 °C. The pressure, gas flow rate, and time were kept constant between annealing experiments.

In the first set: annealing was performed at four temperatures: 900 °C, 950 °C, 970 °C, and 980 °C/1,000 °C temperature variations. For each annealing experiment, the annealing time, pressure, and flow ratio were kept constant. Figure 7 shows the surface of 99.999 % copper foil after annealing at different temperatures. From this set, it is observed that annealing under 970 °C produced the smoothest surface. Higher temperatures of 980 °C and 1,000 °C produced a rougher surface due to excess evaporation of copper. Conversely, the substrate annealed at a lower

temperature of 900 °C did not show any significant changes in the surfaces, indicating that more energy or time is necessary to achieve surface modification.

In the second experimental set, the effect of annealing time was investigated: four different annealing times from 40 to 120 minutes were selected while the other parameters, such as the temperature, the pressure, and the gas flow rates were kept constant at 970 °C, 200 – 350 mTorr, and 5:2 sccm flow of Ar: H_2 respectively. Figure 8 shows that as the annealing time was increased, the copper surface becomes smoother with the best results obtained for 120 minutes.

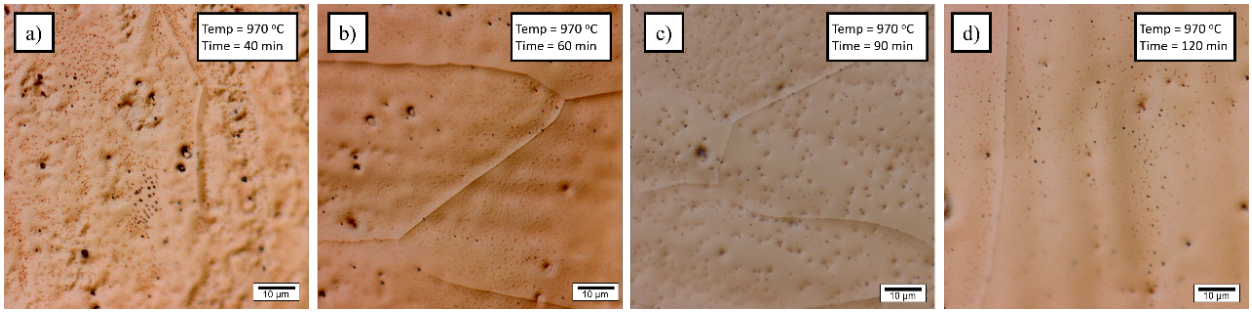

Figure 8. Copper foil substrates after annealing experiments at different times: (a) 40, (b) 60, (c) 90 and (d) 120 minutes. The pressure, gas flow rate, and temperature were kept constant for the annealing experiments.

From these two experimental sets, the best copper surface, as signified by the lowest surface roughness and the largest Cu grain size, was achieved at 970 °C for 120 minutes (Figure 4d). All experimental conditions and optical images of the annealed substrates are summarized in Table 1 and Figure B of the Appendix.

c) Graphene growth results

Three sets of graphene growth experiments were performed. In each experiment set, one of three parameters, (1) time, (2) pressure, or (3) gas (CH_4 and H_2) flow rates were optimized, while the other two were kept constant. Table 2 summarizes all parameters used in the growth experiments labeled with a code (E#).

In the first experimental set, the graphene growth time was varied from 30 to 40 minutes, while keeping the gas flow rates (CH_4: 5 sccm and H_2: 2 sccm), temperature (995 °C), and pressure (~500 mTorr) constant. The optical images in Figures 9a and 9b show that the surface is visibly smoother on the 30-minute growth (E18) film than the 40-minute growth (E15) film. Additionally, the Raman spectra in Figures 9c and 9d show that graphene growth occurs only for the 30-minute growth. The Raman analysis confirms that the E18 sample (Figure 9d) shows peaks at 2730 cm^{-1} and at 1600 cm^{-1}, which correspond to characteristic graphene 2D and G peaks. Additionally, the defect D peak that appears around 1,350 cm^{-1} was not observed for the E18 sample, indicating that the graphene film is free of defects. The Raman spectrum for experiment E15 in Figure 9c, however, does not show any signature graphene peaks confirming the lack of graphene growth.

Table 2. Growth experiments using the optimized annealing step conditions

EXP	Gas Flow (sccm)		Temperature (°C)	Time (min)	Pressure (mTorr)
	CH_4	H_2			
E11	5	2	980	60	343-500
E12	5	2	995	30	337-321
E13	5	2	1005	30	203-490
E14	5	2	1015	30	328-492
E15	5	2	995	40	325-489
E16	5	2	995	30	337-488
E17	5	2	995	30	351-525
E18	5	2	995	30	350-530
E19	6	1	995	30	350-552
E20	5	2	995	30	350-558
E21	6	2	995	30	358-575
E22	7	2	995	30	357-600
E23	6	2	995	30	357-586
E24	6	2	995	30	350-592

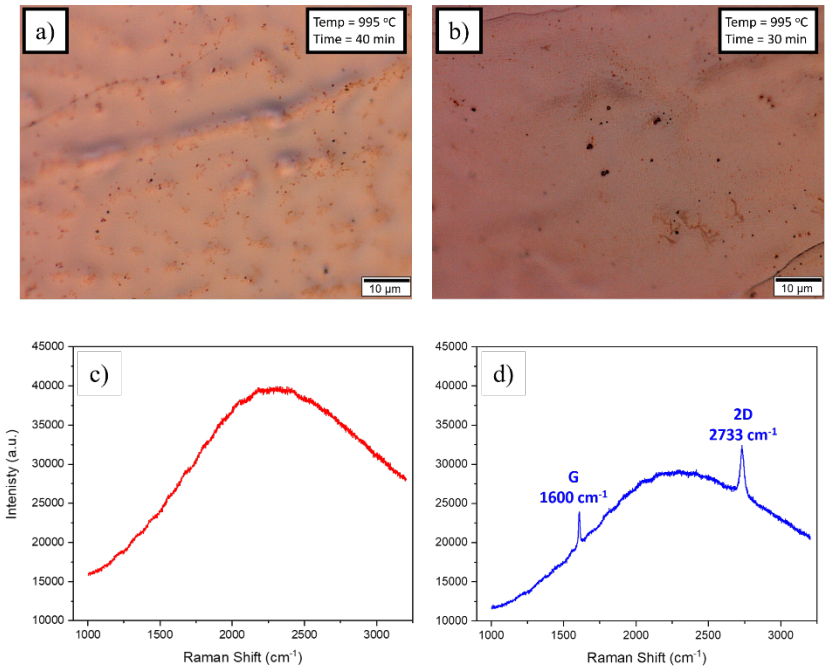

Figure 9. Optical images and Raman measurements of graphene growth at a different times, keeping the other parameters constant (temperature of 995 °C, pressure of 500 mTorr, gas flow rates of 5 sccm, and 2 sccm for CH_4 and H_2 respectively). Figures (a) and (b) show the optical images of samples E15 and E18. Figures (c) and (d) represent the Raman spectra corresponding to these samples.

In the second experiment set, the flow rates of methane (CH_4) and hydrogen (H_2) were varied while keeping the temperature of 995°C, time of 30 minutes, and the pressure in the ~500–600 mTorr range constant. Four experiments (E18 – E22) were conducted. The methane and hydrogen gas flows were varied from 5 to 7 sccm and from 1 to 2 sccm for methane and hydrogen, respectively. Figure 10 indicates that the smoothest surface was obtained under two flow rate conditions: the first one at 5:2 sccm CH_4:H_2 (Figure 10a, E18), and the second at 6:2 sccm CH_4:H_2 (Figure 10c, E21) flow rates. In contrast, flow rates of 6:1 sccm (Figure 9b, E19) and 7:2 sccm of CH_4:H_2 (Figure 10d, E22) produced rougher surfaces. Additionally, Raman analysis shows that graphene was present on the smoother samples of E18 and E21 (Figure 10e and 10g) while it was absent in the rough sample E19 (Figure 10f). Surprisingly, one rough surface in E22 (Figure 10h) exhibited the signature graphene peaks indicating carbon nucleation from a high level of methane gas.

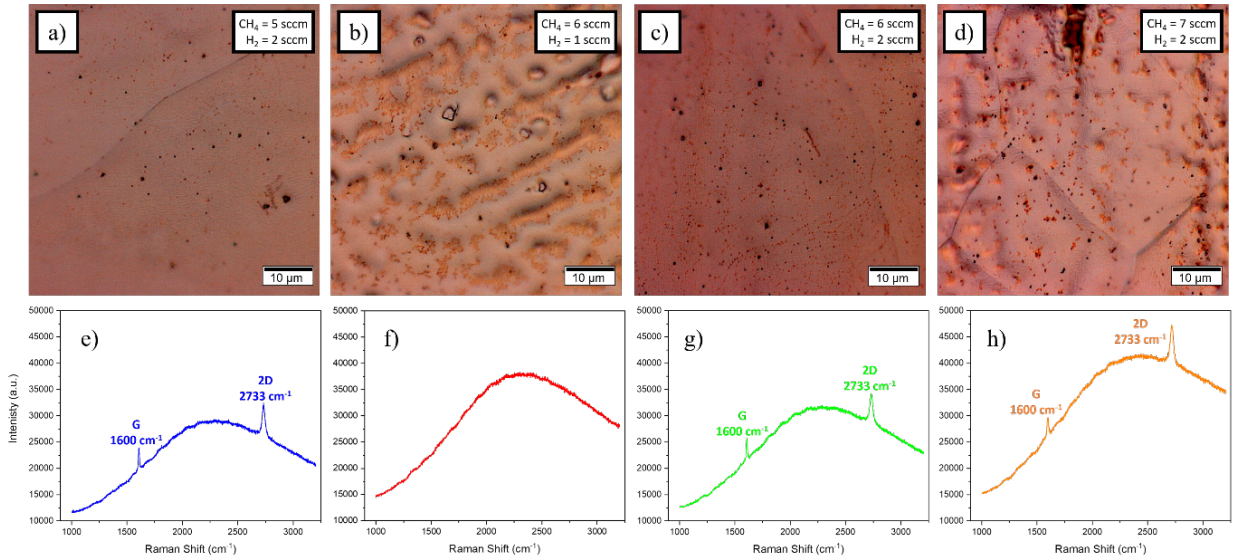

Figure 10. Optical images and Raman measurements of graphene grown at different gas flow rates (CH_4 and H_2) while keeping the other parameters constant (growth temperature of 995 ºC, pressure of ~ 500mTorr, and reaction time of 30 minutes). The gas flow rates were: (a) 5:2 sccm, CH_4:H_2, (b) 6:1 sccm, CH_4:H_2, (c) 6:2 sccm, CH_4:H_2, and (d) 7:2 sccm, CH_4:H_2. Figures (e), (f), (g), and (h) represent the Raman measurements of the corresponding images.

In the third experimental set, the growth temperature was varied from 995 °C to 1,015 °C, while keeping the other optimized parameters constant: gas flow rates (5 sccm and two sccm for CH_4 and H_2 respectively), growth time (30 minutes) and pressure (~500 mTorr). Three experiments (E13, E14, and E18) were conducted. The results indicate that the graphene growth at 995 °C (Figure 11a, E18) produced the smoothest and most continuous graphene film growth compared to the higher temperatures of 1,005 °C and 1,015 °C (Figures 11b and 11c, E13 and E14). Additionally, Raman analysis shows that growth at temperatures of 1,005 ºC and 1,015 ºC (Figures 11e and 11f) did not produce any graphene. The lack of development at higher temperatures (>1,000 ºC) can be attributed to a phase change (melting) of the copper metal (Figure 3) near the material's melting temperature.

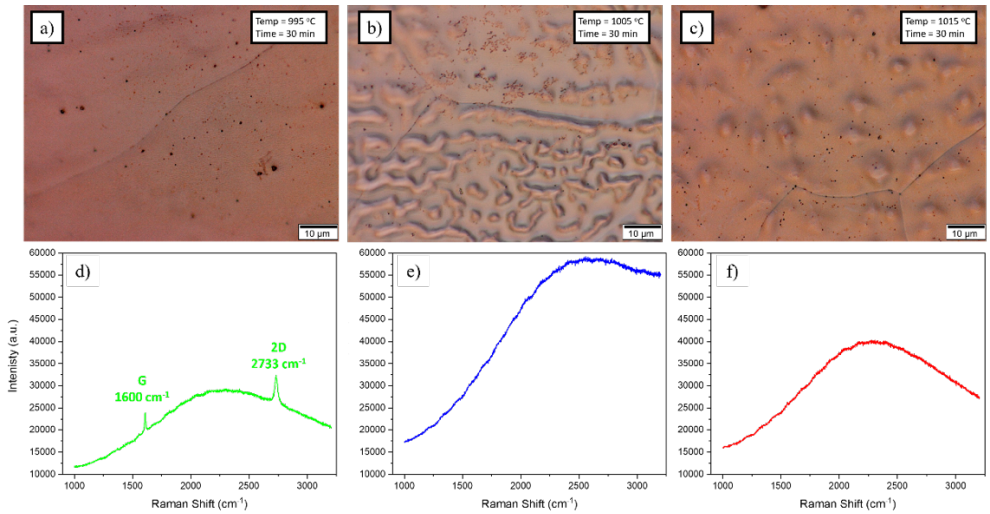

Figure 11. Optical images and Raman measurements of graphene grown at different temperatures (995 ºC, 1,005 ºC, and 1,015 ºC) while keeping other parameters constant (pressure of ~500 mTorr, reaction time of 30 minutes, and gas flow rates of 5 and 2 sccm for CH_4 and H_2 respectively.). Where (a), (b), and (c) are the optical images of samples at 995 °C, 1,000 °C, and 1,015 °C (E18, E13, E14), respectively. Figure (d), (e), and (f) represent the Raman spectra corresponding to these samples.

In summary, after conducting three sets of growth experiments, the optimal graphene growth conditions for our CVD system were determined: growth temperature of 995 ºC, growth time of 30 minutes, gas flow rate ratios (CH_4:H_2) of 5:2, and ~ 500 mTorr of internal chamber pressure. A schematic of the optimized overall synthesis process, including annealing, growth, and cooling steps is depicted in Figure 12. Optical images of all experimental conditions summarized in Table 3 are presented in Appendix D.

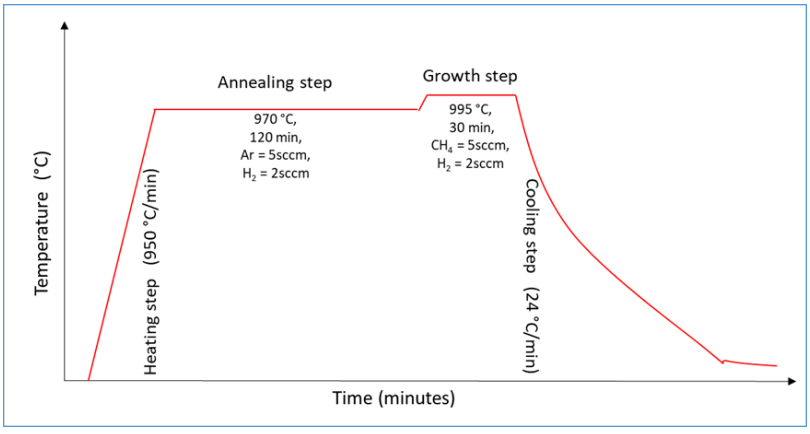

Figure 12. Optimized graphene synthesis parameters on copper substrates by CVD: heating, annealing, growth, and cooling steps with corresponding temperature, time, and gas flow profile.

Upon graphene growth optimization, the differences in the effect of substrate purity on graphene growth were investigated. So far, the presented results were obtained from commercially available, highest purity 99.999 % copper substrates. Herein, a 99.8 % purity copper substrate was utilized for graphene growth. Applying the same optimized conditions as described in Figure 12 indicated that a different graphene growth pattern resulted on the 99.8 % purity copper substrate. As observed in Figure 13, higher, the 99.999 % purity substrate resulted in the continuous growth of graphene (Figure 13a) while discontinuous, star-shaped growth was obtained from the 99.8 % purity copper substrate (Figure 13b). The discontinuous, star-shaped growth can be attributed to the presence of more crystalline defects on the lower purity substrate resulting in intermittent nucleation sites as well as discontinuities during the expansion phase due to the substrate-related defects compared to more crystalline higher purity substrate.

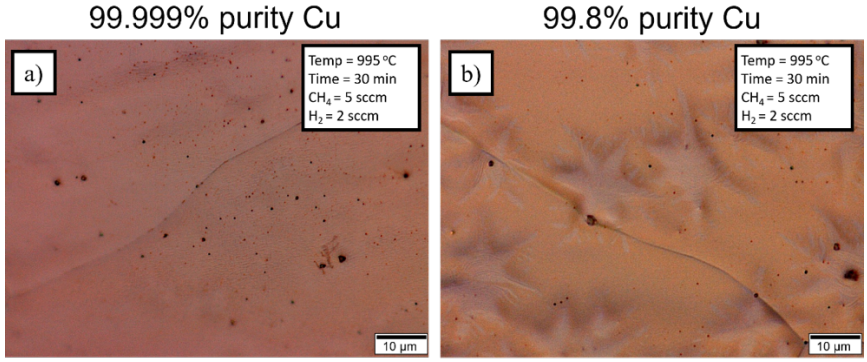

Figure 13. Optical images of graphene films grown on copper foil substrates on (a) high 99.999 % purity, and (b) lower, 99.8 % purity copper substrates. Both growths were performed at the same optimized annealing and growth conditions showing different growth patterns.

Furthermore, Figure 14 shows optical images of both top and the bottom sides of graphene grown on the 99.8 % copper substrate. In comparing the two sides, the top facet (Figure 14a) shows a discontinuous star-shaped pattern a few tens of microns in size, while the bottom facet (Figure 14b) shows a more continuous snowflake-like growth pattern. Additional optical images in Appendix E show graphene grain boundaries of varying size on the bottom face. The difference in growth pattern is attributed to the exposure of the substrate faces with respect to the hydrocarbon and carrier gases. As the substrate was placed on the sample holder without any mounts to keep it in place, only the top face of the substrate was exposed to the hydrocarbon gas resulting in the consistent growth of the star-shaped graphene. Additionally, due to the substrate placement geometry, the exposed area of the bottom side varied from experiment to experiment due to factors such as the curvature of the substrate and the effect of gas flow resulting in inconsistent exposure to the bottom side between experiments.

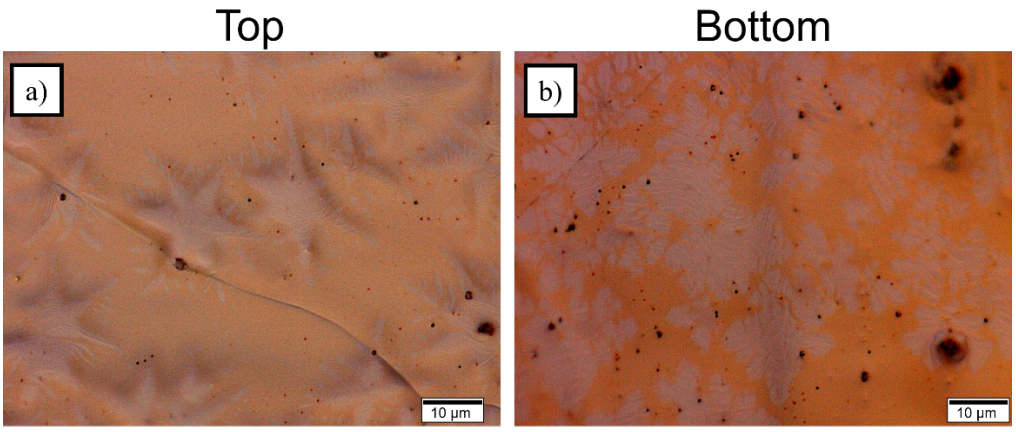

Figure 14. Optical images of the graphene films on (a) top (exposed to gas flow) and (b) bottom (not exposed to gas flow) of a 99.8 % purity copper substrate showing discontinuous graphene growth with star shape on the top and snowflake shape growth on the bottom.

While successful optimization for low-pressure chemical vapor deposition of graphene was achieved, further optimization with the goal of (1) investigating the effect of Cu surface to direct versus indirect gas flow exposure and (2) removing black particles on the graphene-Cu foil post-growth is discussed herein.

Graphene growth on copper substrates utilizing optimized conditions in Figure 12 indicates defect-free growth (confirmed by Raman spectroscopy) on both high (99.999 %) and lower (99.8 %) purity substrates. However, high density areas of black particles and impurities were observed on surface of both types of copper substrates after graphene growth. These particles may cause the graphene film to tear during transfer and thus should be minimized. The absence of the D peak indicated that these particles were linked to the Cu foil substrate itself. Unlike white particles on copper surfaces from quartz tube impurities,[57] black particles might indicate the presence of copper oxide. Even though no study was conducted to verify the composition as these black particles in this report, an indirect verification was obtained when an electropolished Cu foil was used as a growth substrate.

It is well known that electropolishing Cu foils not only reduces the roughness of the surface but also removes some of the copper oxide impurities. Figures 15a and 15b show untreated and electropolished copper surfaces (99.8 % purity) prior to graphene growth, while Figures 15c and 15d show the copper substrate after graphene growth on unpolished and electropolished substrates. In comparing figures 15a and 15b, the electropolished substrate shows a significant reduction in black impurities. Conversely, Figure 15c illustrates that black contaminants are still present on unpolished copper substrate after graphene growth. Additionally, as the copper substrate is lower purity, the resulting graphene growth is discontinuous with a star-like pattern, as seen in Figure 13. Conversely, graphene growth on the electropolished copper foil (figure 15d) yielded graphene films with no visible impurities indicating that electropolishing of the copper substrate surface results in significant improvement in graphene growth quality, even for lower purity substrates.

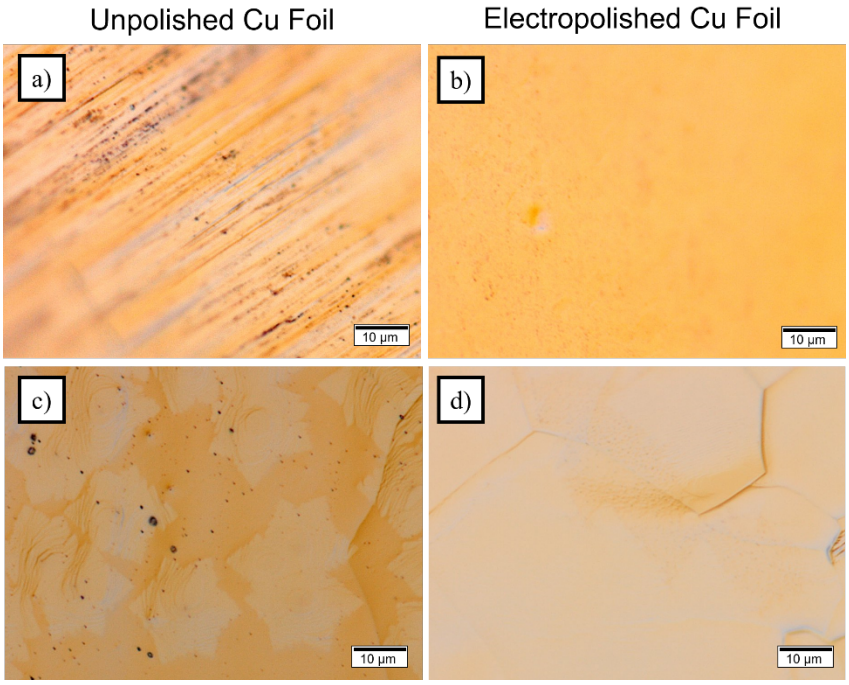

Figure 15. Optical images of the graphene films grown on unpolished and electropolished copper foil, where (a) and (b) correspond to substrates before growth while (c) and (d) shows substrates post-graphene growth on (c) unpolished, and (d) electropolished copper substrates respectively.

Next, the effect of substrate orientation with respect to exposure to the gas flow was investigated using three different substrate orientations, as shown in Figure 16: (1) Regular, (2) Ceramic standoff, and (3) Cu foil wrapping. In the typical setup, as seen in Figure 16a, the copper substrate was placed on the sample holder with only the top surface of the Cu foil substrate exposed directly to the gas flow. In the ceramic standoff setup (Figure 16b), the substrate was placed on top of two ceramic pillars - with both surfaces of the Cu foil exposed to the gas flow - the top one directly and the bottom exposed indirectly. Lastly, in the Cu wrapping setup (Figure 16c), the copper substrate was placed on the substrate holder, then wrapped with a different Cu foil. In this case, the Cu foil growth substrate was exposed indirectly to the gas flow, and we hypothesize that the actual gas flow rate on the substrate is much lower than the typical case described in Figure 16a.

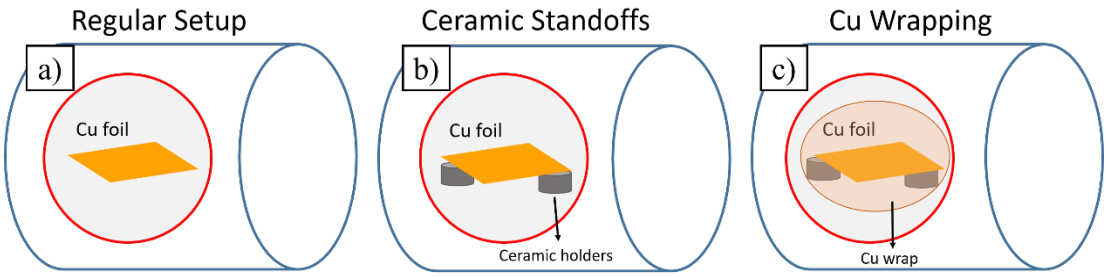

Figure 16. Graphene growth experiments for different conditions: (a) typical, (b) ceramic standoff, and (c) wrapping. The red circle represents the sample holder in which the substrate and ceramic holders are placed.

Optical images of graphene films on Cu foils utilizing the three setups (Figure 16) are shown in Figure 17. In the typical setup (Figures 17a and 17d), when only the top surface of the Cu foil is exposed to gas flow, a continuous graphene film was observed on the top face. Meanwhile, individual grains of several tens of microns were present on the bottom. Additionally, black impurities were observed on both the top and bottom sides. This was not unexpected because while the copper substrate is the highest purity (99.999 %), the substrate was not electropolished to improve the substrate surface. In the ceramic standoff setup (Figures 17b and 17e), the graphene film surfaces were rougher compared to the previous case with continuous growth on both top and the bottom of the foil as the gases have access to both sides of the copper foil. Finally, in the Cu wrap setup, the graphene film surfaces (Figures 17c and 16f) were similar in roughness to the standard method. However, larger grain size/more continuous films were detected on the bottom side in the Cu wrapping method compared to the standard process. Furthermore, the Cu wrapping method reduced the amount of copper oxide impurities compared to the standard setup. Thus, these results indicate that graphene film growth on copper foil using the Cu wrap setup is the best growth approach because it produced both the smoothest and the cleanest graphene.

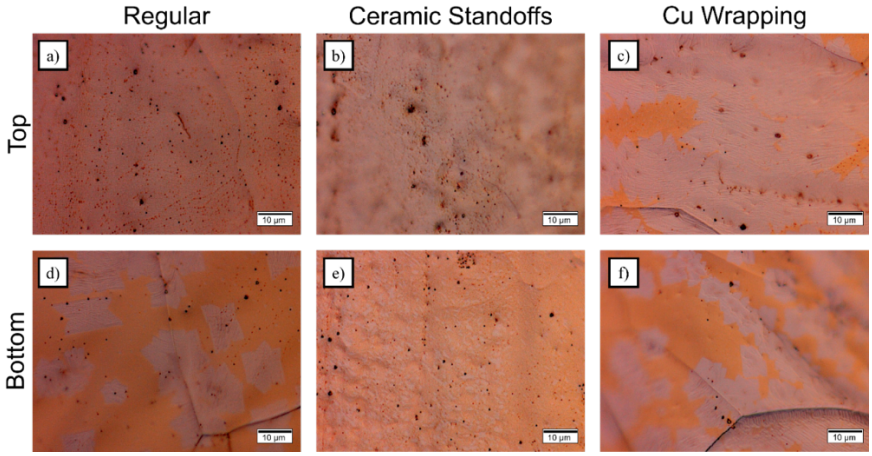

Figure 17. Optical images of the top and bottom of the sample for different setups: regular, ceramic standoffs, and wrapping. (a), (b) and (c) indicate the top of the foil while (d), (e), and (f) show corresponding bottom surfaces.

Lastly, the Cu wrapping method was utilized with a 99.999 % untreated and an electropolished 99.8 % purity substrates. The Raman and optical microscope analyses are shown in Figures 18 and 19, respectively. The Raman analysis showed high-quality graphene was produced in both cases. However, the optical images show that while Cu wrapping indeed reduces black oxide impurities, the combination of Cu wrapping with electropolishing almost eliminates copper oxide impurities. Additional experiments will be conducted for further graphene film characterization and transfer to inorganic and organic materials.

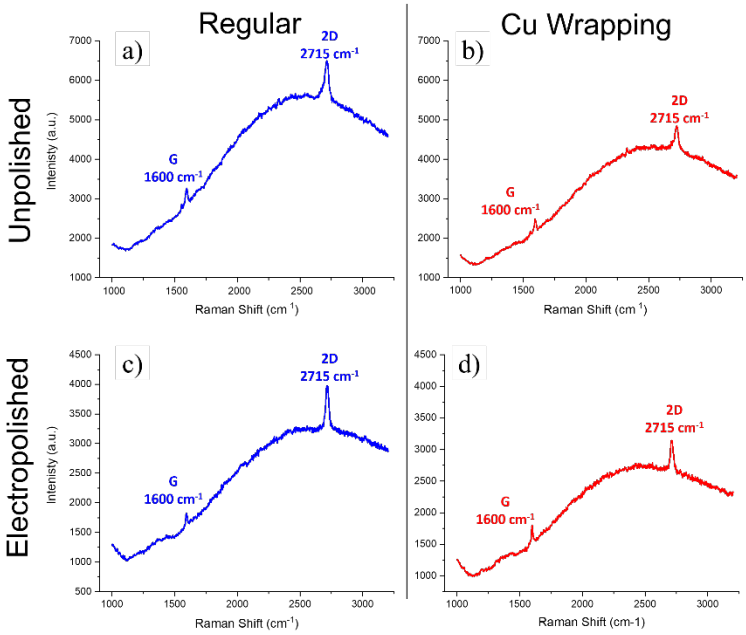

Figure 18. Raman spectra for graphene on unpolished and electropolished substrates using the regular and copper foil wrap setups. Where (a) and (c) show unpolished and electropolished samples in the typical setup while (b) and (d) show unpolished and electropolished substrates in the wrapping setup.

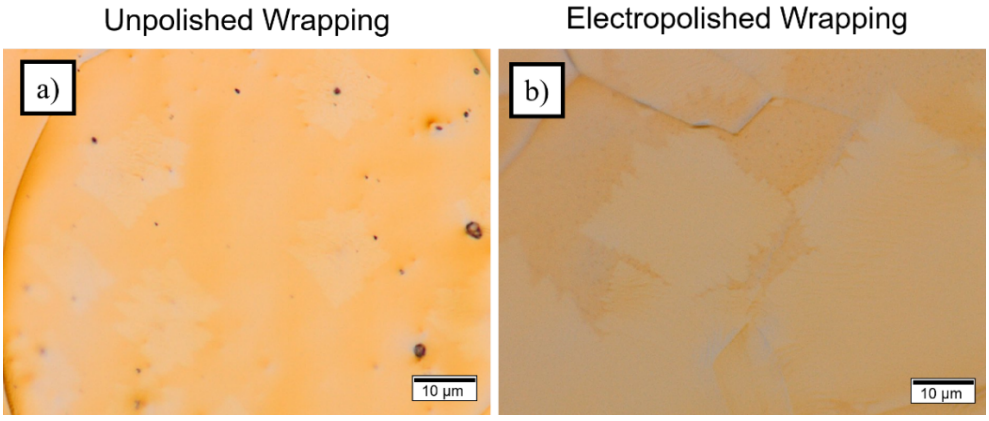

Figure 19. Optical images of graphene grown via the wrapping setup shows graphene grown on (a) an unpolished substrate while (b) shows graphene grown on an electropolished substrate.

IV. Summary

A systematic approach for growing large-area graphene films on copper foils in a low-pressure chemical vapor deposition (LPCVD) system was developed. The copper substrate purity, subsequent treatments (chemical or electropolishing), the placement and the orientation of the substrate in the CVD reactor, and experimental parameters affected the growth and quality of the graphene films. The synthesized graphene utilizing optimized parameters produced high-quality, defect-free graphene films on a 1x1 cm^2 copper substrate verified by both optical microscopy and Raman spectroscopy. Additionally, using the same optimized conditions on a lower purity, 99.8 % copper substrate, a discontinuous, star-shaped growth on the top surface, and snowflake-like film growth on the bottom surface were observed. Additional electropolishing of the surface and Cu foil wrapping of the substrate during the growth step was utilized to improve the graphene quality further by reducing the amount of substrate related copper oxide impurities. Although the detailed mechanisms responsible for the different graphene growth shapes and quality with various modifications are not yet fully understood, this work provides a basis for the high-quality, continuous growth of wafer-scale graphene films for the development of graphene enabled optoelectronic and quantum technology.

References

1. Berger, C. Electronic Confinement and Coherence in Patterned Epitaxial Graphene. *Science* **312**, 1191 (2006).
2. Ihnatsenka, S., Zozoulenko, I. V. & Kirczenow, G. Band-gap engineering and ballistic transport in edge-corrugated graphene nanoribbons. *Phys. Rev. B - Condens. Matter Mater. Phys.* **80**, 1 (2009).
3. Goossens, S. *et al.* Broadband image sensor array based on graphene-CMOS integration. *Nat. Photonics* **11**, 366 (2017).
4. Kong, W. *et al.* Path towards graphene commercialization from lab to market. *Nat. Nanotechnol.* **14**, 927 (2019).
5. Das, T. *et al.* Vertical field effect tunneling transistor based on graphene-ultrathin Si nanomembrane heterostructures. *2D Mater.* **2**, 44006 (2015).
6. Wang, J., Han, J., Chen, X. & Wang, X. Design strategies for two-dimensional material photodetectors to enhance device performance. *InfoMat.* **1**, 33 (2019).
7. Shin, D. H. & Choi, S. H. Graphene-based semiconductor heterostructures for photodetectors. *Micromachines* **9**, 350 (2018).
8. Nguyen, B. H. & Nguyen, V. H. Advances in graphene-based optoelectronics, plasmonics and photonics. *Adv. Nat. Sci. Nanosci. Nanotechnol.* **7**, 13002 (2016).
9. Luo, S., Wang, Y., Tong, X. & Wang, Z. Graphene-based optical modulators. *Nanoscale Res. Lett.* **10**, 199 (2015).
10. Mittendorff, M., Li, S. & Murphy, T. E. Graphene-Based Waveguide-Integrated Terahertz Modulator. *ACS Photonics* **4**, 316 (2017).
11. Guo, J. *et al.* High-performance silicon−graphene hybrid plasmonic waveguide photodetectors beyond 1.55 μm. *Light Sci. Appl.* **9**, 29 (2020).
12. Polat, E. O. *et al.* Synthesis of Large Area Graphene for High Performance in Flexible Optoelectronic Devices. *Sci. Rep.* **5**, 1 (2015).
13. Karimi, K., Jabari, E., Toyserkani, E. & Lee-Sullivan, P. Highly conductive graphene paper for flexible electronics applications. *J. Mater. Sci. Mater. Electron.* **29**, 2537 (2018).
14. Mahmoudi, T., Wang, Y. & Hahn, Y. B. Graphene and its derivatives for solar cells application. *Nano Energy* **47**, 51 (2018).
15. O'Keeffe, P. *et al.* Graphene-Induced Improvements of Perovskite Solar Cell Stability: Effects on Hot-Carriers. *Nano Lett.* **19**, 684 (2019).
16. Randviir, E. P., Brownson, D. A. C. & Banks, C. E. A decade of graphene research: Production, applications and outlook. *Mater. Today* **17**, 426 (2014).
17. Das, S., Pandey, D., Thomas, J. & Roy, T. The Role of Graphene and Other 2D Materials in Solar Photovoltaics. *Adv. Mater.* **31**, 1 (2019).
18. Cheng, Q. *et al.* Graphene-Like-Graphite as Fast-Chargeable and High-Capacity Anode Materials for Lithium Ion Batteries. *Sci. Rep.* **7**, 1 (2017).
19. Peña-Bahamonde, J., Nguyen, H. N., Fanourakis, S. K. & Rodrigues, D. F. Recent advances in graphene-based biosensor technology with applications in life sciences. *J. Nanobiotechnology* **16**, 1 (2018).
20. Kim, J., Kim, S. & Jung, W. Highly enhanced compatibility of human brain vascular pericyte cells on monolayer graphene. *Bioengineered* **8**, 85 (2017).
21. Tehrani, Z. *et al.* Generic epitaxial graphene biosensors for ultrasensitive detection of cancer risk biomarker. *2D Mater.* **1**, 025004 (2014).

22. Hwang, M. T. *et al.* Ultrasensitive detection of nucleic acids using deformed graphene channel field effect biosensors. *Nat. Commun.* **11**, 1543 (2020).
23. Coroş, M., Pruneanu, S. & Stefan-van Staden, R.-I. Review—Recent Progress in the Graphene-Based Electrochemical Sensors and Biosensors. *J. Electrochem. Soc.* **167**, 037528 (2020).
24. Novoselov, K. S. *et al.* Electric field in atomically thin carbon films. *Science* **306**, 666 (2004).
25. Nepal, A., Singh, G. P., Flanders, B. N. & Sorensen, C. M. One-step synthesis of graphene via catalyst-free gas-phase hydrocarbon detonation. *Nanotechnology* **24**, 245602 (2013).
26. Lin, Y. *et al.* 100-GHz Transistors from Wafer-Scale Epitaxial Graphene. *Science* **327**, 662 (2010).
27. Kim, K. S. *et al.* Large-scale pattern growth of graphene films for stretchable transparent electrodes. *Nature* **457**, 706 (2009).
28. Li, X. *et al.* Large-area synthesis of high-quality and uniform graphene films on copper foils. *Science* **324**, 1312 (2009).
29. Zhang, J. *et al.* Synthesis of graphene from dry ice in flames and its application in supercapacitors. *Chem. Phys. Lett.* **591**, 78 (2014).
30. Chakrabarti, A. *et al.* Conversion of carbon dioxide to few-layer graphene. *J. Mater. Chem.* **21**, 9491 (2011).
31. Ponomarenko, L. A. *et al.* Chaotic dirac billiard in graphene quantum dots. *Science* **320**, 356 (2008).
32. Badami, D. V. Graphitization of α-Silicon Carbide. *Nature* **193**, 569 (1962).
33. Malesevic, A. *et al.* Synthesis of few-layer graphene via microwave plasma-enhanced chemical vapour deposition. *Nanotechnology* **19**, 305604 (2008).
34. Subrahmanyam, K. S., Panchakarla, L. S., Govindaraj, A. & Rao, C. N. R. Simple method of preparing graphene flakes by an arc-discharge method. *J. Phys. Chem. C* **113**, 4257 (2009).
35. Muñoz, R. & Gómez-Aleixandre, C. Review of CVD synthesis of graphene. *Chem. Vap. Depos.* **19**, 297 (2013).
36. Bhaviripudi, S., Jia, X., Dresselhaus, M. S. & Kong, J. Role of kinetic factors in chemical vapor deposition synthesis of uniform large area graphene using copper catalyst. *Nano Lett.* **10**, 4128 (2010).
37. Chen, X., Zhang, L. & Chen, S. Large area CVD growth of graphene. *Synth. Met.* **210**, 95–108 (2015).
38. Seah, C. M., Chai, S. P. & Mohamed, A. R. Mechanisms of graphene growth by chemical vapour deposition on transition metals. *Carbon* **70**, 1 (2014).
39. López, G. A. & Mittemeijer, E. J. The solubility of C in solid Cu. *Scr. Mater.* **51**, 1 (2004).
40. Yang, R. T., Goethel, P. J., Schwartz, J. M. & Lund, C. R. F. Solubility and diffusivity of carbon in metals. *J. Catal.* **122**, 206 (1990).
41. Oshima, C. & Nagashima, A. Ultra-thin epitaxial films of graphite and hexagonal boron nitride on solid surfaces. *J. Phys. Condens. Matter* **9**, 1 (1997).
42. Campos-Delgado, J. *et al.* CVD synthesis of mono- and few-layer graphene using alcohols at low hydrogen concentration and atmospheric pressure. *Chem. Phys. Lett.* **584**, 142 (2013).
43. No, Y. S. *et al.* Layer number identification of CVD-grown multilayer graphene using Si peak analysis. *Sci. Rep.* **8**, 1 (2018).

44. Yan, Z. *et al.* Toward the Synthesis of Wafer-Scale Single-Crystal Graphene on Copper Foil. *ACS Nano* **6**, 9110–9117 (2012).
45. Antonova, I. V. Chemical vapor deposition growth of graphene on copper substrates: current trends. *Physics-Uspekhi* **56**, 1013 (2013).
46. Li, X. *et al.* Large-area graphene single crystals grown by low-pressure chemical vapor deposition of methane on copper. *J. Am. Chem. Soc.* **133**, 2816 (2011).
47. Li, X. *et al.* Graphene films with large domain size by a two-step chemical vapor deposition process. *Nano Lett.* **10**, 4328 (2010).
48. Wofford, J. M., Nie, S., McCarty, K. F., Bartelt, N. C. & Dubon, O. D. Graphene Islands on Cu Foils: The Interplay between Shape, Orientation, and Defects. *Nano Lett.* **10**, 4890 (2010).
49. Guermoune, A. *et al.* Chemical vapor deposition synthesis of graphene on copper with methanol, ethanol, and propanol precursors. *Carbon* **49**, 4204 (2011).
50. Cortés, A., Celedón, C. & Zarate, R. CVD synthesis of graphene from acetylene catalyzed by a reduced CuO thin film deposited on SiO_2 substrates. *J. Chil. Chem. Soc.* **60**, 2911 (2015).
51. Yao, Y. *et al.* Controlled growth of multilayer, few-layer, and single-layer graphene on metal substrates. *J. Phys. Chem. C* **115**, 5232 (2011).
52. Li, Z. *et al.* Low-temperature growth of graphene by chemical vapor deposition using solid and liquid carbon sources. *ACS Nano* **5**, 3385 (2011).
53. Ruan, G., Sun, Z., Peng, Z. & Tour, J. M. Growth of graphene from food, insects, and waste. *ACS Nano* **5**, 7601 (2011).
54. Vlassiouk, I. *et al.* Role of hydrogen in chemical vapor deposition growth of large single-crystal graphene. *ACS Nano* **5**, 6069 (2011).
55. Choi, D. S. *et al.* Effect of cooling condition on chemical vapor deposition synthesis of graphene on copper catalyst. *ACS Appl. Mater. Interfaces* **6**, 19574 (2014).
56. Seo, J. *et al.* Study of Cooling Rate on the Growth of Graphene via Chemical Vapor Deposition. *Chem. Mater.* **29**, 4202 (2017).
57. Al-Kamiyani, S. & Mohiuddin, T. Improved control in elimination of white impurities on graphene by chemical vapor deposition (CVD). *AIP Adv.* **8**, 125325 (2018).

Appendix

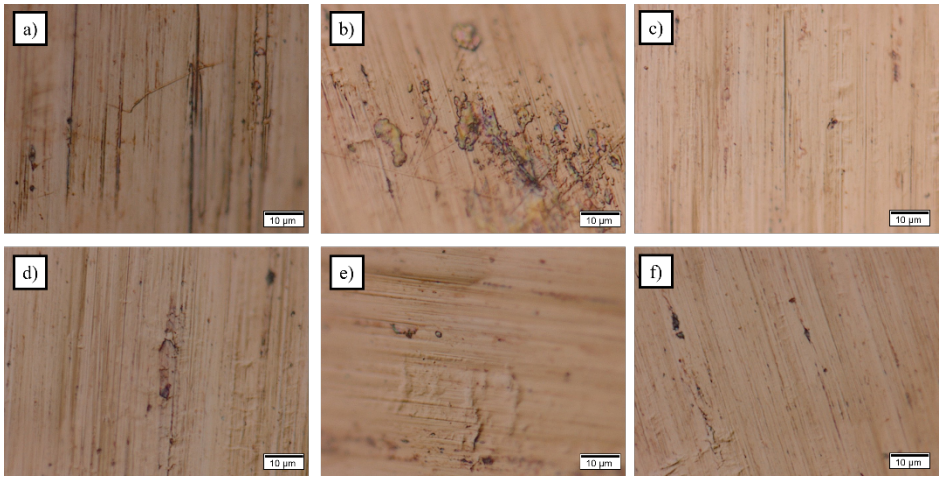

Figure A. Copper foil with 99.999 % purity before annealing treatment (magnification 100x for all samples).

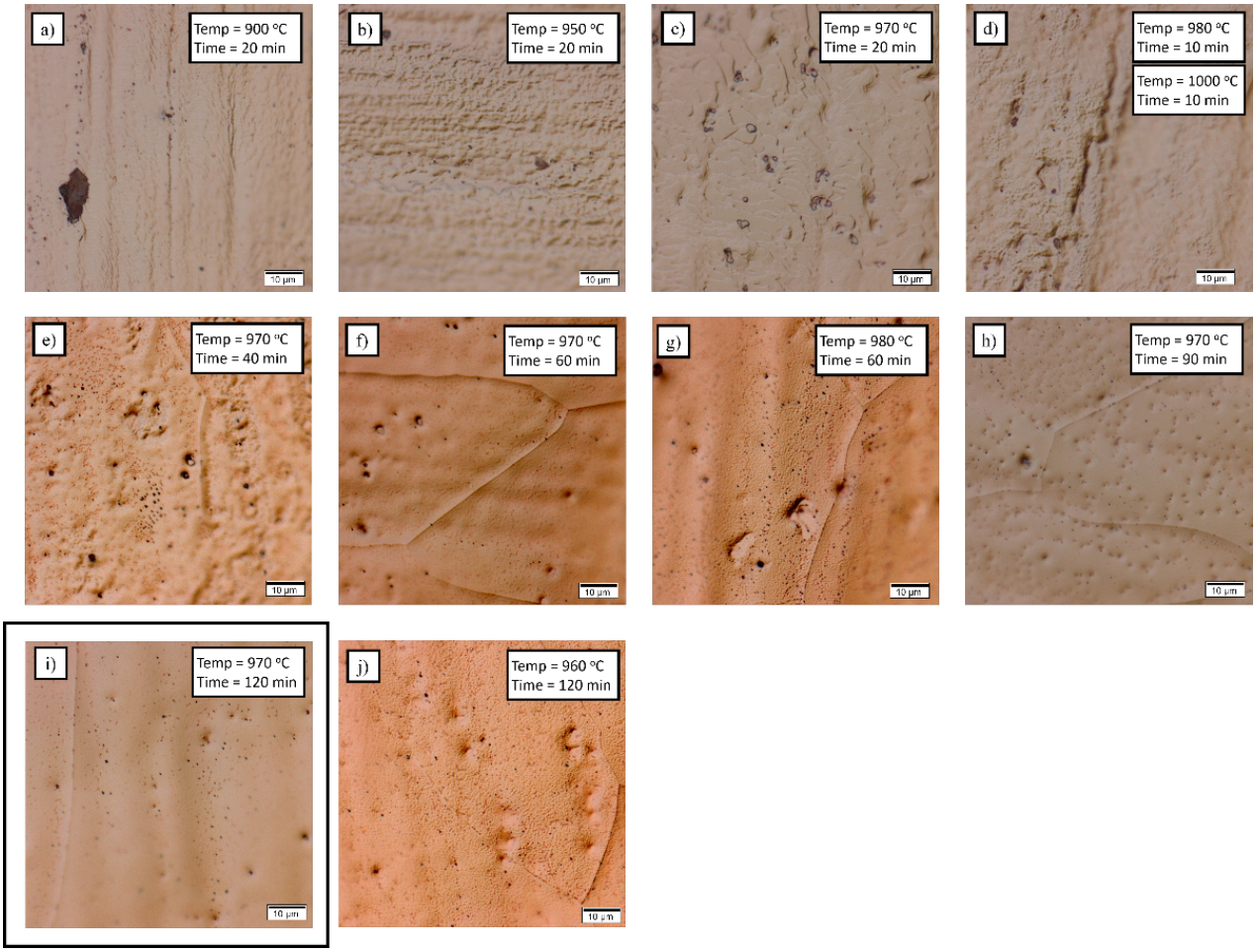

Figure B. Annealing experiments at different times and temperatures, where the best annealing (smoothest copper surface) is shown in (i), at 970 ºC for 120 minutes.

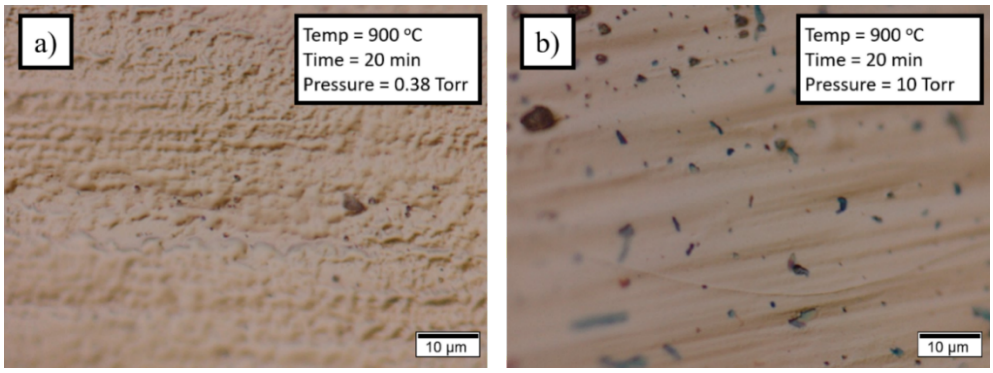

Figure C. Annealing experiments at different pressures; (a) 0.38 Torr, and (b) 10 Torr. The anneal time, temperature, and gas flow was kept constant (growth time 20 minutes, the growth temperature of 900 °C, gas flows of 5 sccm and 2 sccm for Ar and H_2 respectively).

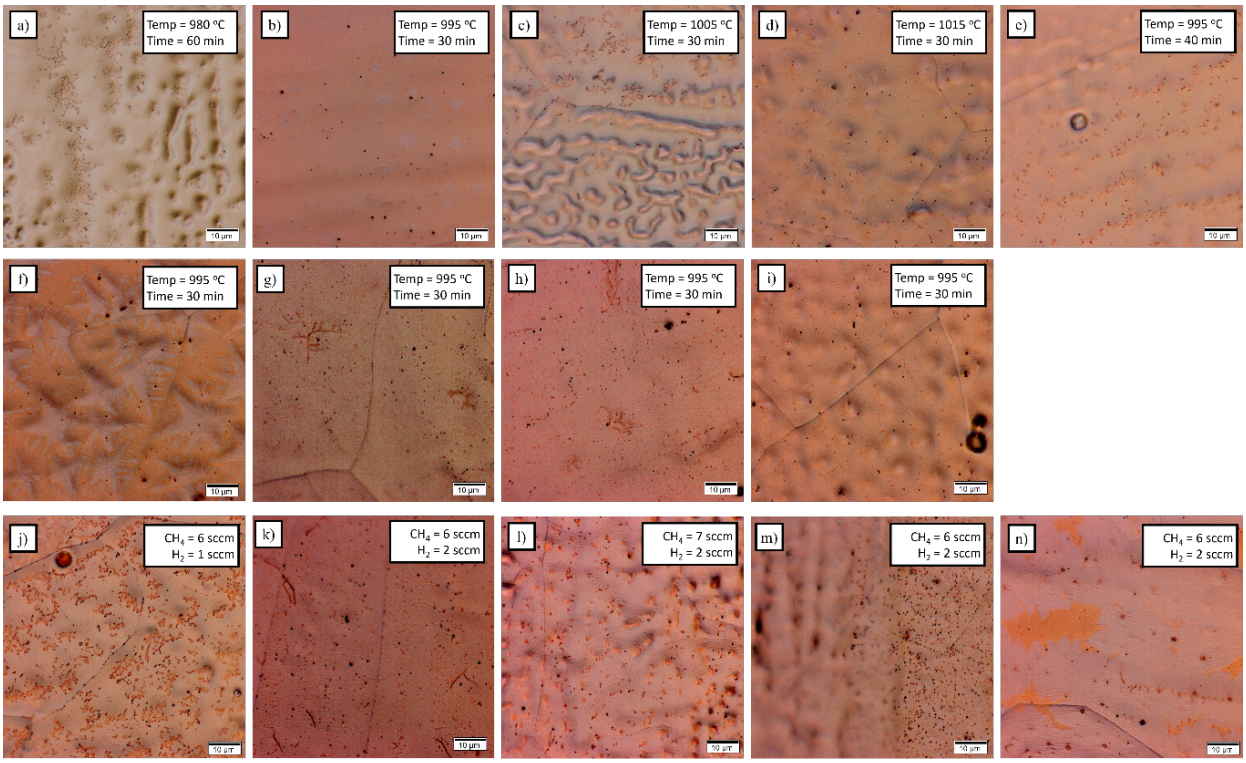

Figure D. Graphene growth experiments with the optimized annealing condition. Figures (a) – (i) were conducted under the constant gas flow (5 and 2 sccm for CH_4 and H_2) with varying temperature and time. Figures (j) – (n) were conducted under constant temperature and time (995 °C for 30 minutes) while varying the gas flow.

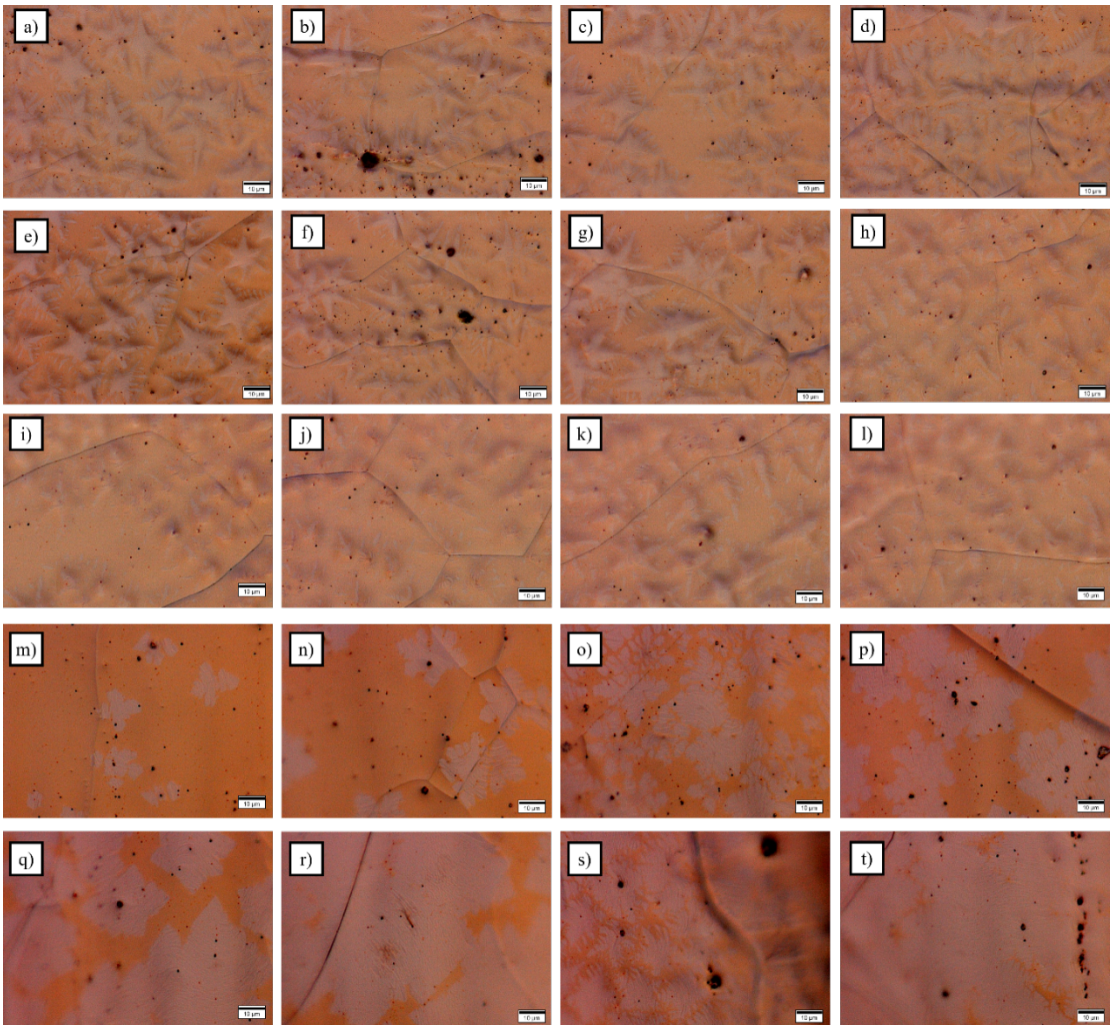

Figure E. Growth experiments for optimized annealing, and growth conditions on lower purity, 99.8 % copper substrate. (a) – (l) show the top side in which distinct star-shaped growth is observed. The dimensions of the star-shape growth are consistent throughout the experiments around 30 – 50 µm. (m) – (t) show the bottom side in which snowflake like patterns are observed. Grain size for the bottom side ranges from 10 µm to continuous film growth.

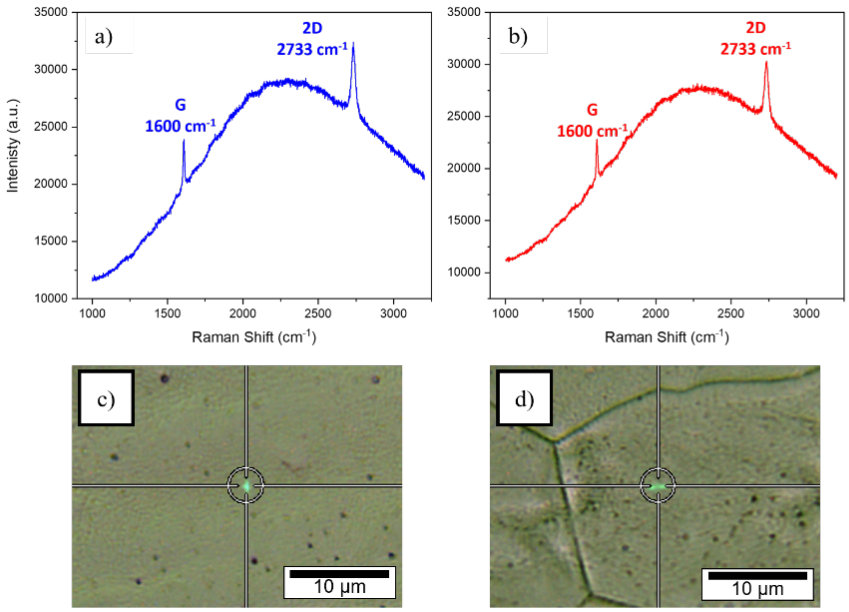

Figure F. Raman spectra for sample E18 (growth temperature of 995 °C, growth time of 30 minutes gas flow rates of 5 sccm and 2 sccm for CH_4 and H_2) at two spot sizes. Where (a) and (b) represent the Raman spectra obtained from spots in (c) and (d), respectively.